Hindawi
Journal of Nanomaterials
Volume 2022, Article ID 4916197, 13 pages
https://doi.org/10.1155/2022/4916197

Research Article

Clothing Nanometer Antimite and Antibacterial Based on Deep Learning Technology

Hai Liu [1,2]

[1]*Department of Big Data, Jiangxi Institute of Fashion Technology, Nanchang, 330201 Jiangxi, China*
[2]*Clothing Big Data Research Center, Jiangxi Institute of Fashion Technology, Nanchang, 330201 Jiangxi, China*

Correspondence should be addressed to Hai Liu; liuhai@jift.edu.cn

Received 19 March 2022; Revised 18 April 2022; Accepted 28 April 2022; Published 18 May 2022

Academic Editor: Awais Ahmed

With the improvement of people's living standards, the living conditions and environment of residents have changed, and there are also more and more electrical appliances such as air conditioners, air purifiers, and humidifiers. People's living environment and office environment are increasingly closed, which makes it easy for mites to breed and multiply. The changes in the living environment have made many people more and more aware of health and safety issues. Under these conditions, it is mainly used in the field of biomedicine. In the high-tech field, nanomaterials with antimite and antibacterial properties have entered the field of clothing and home textiles. With the advancement and development of science and technology, nanomaterial technology tends to mature and becomes a major player in the field of clothing. However, nanosilver alone has some defects, such as large nanoparticles, poor antimite and antibacterial effect, high cost, easy oxidation, and strong toxicity. Therefore, the preparation of new nanocomposite materials is of great significance for the application of nanotechnology to the field of clothing. In this paper, the antimite and antibacterial properties of different nanomaterials on clothing were explored through deep learning technology combined with experimental methods. According to the experiments in this paper, the Ag/TiO_2(ATA) nanocomposites have obvious antibacterial and acarid effects, and the antibacterial and acarid rates are close to 100% under the conditions of visible light and dark light.

1. Introduction

Bacterial mites are ubiquitous organisms in human life. It has strong vitality, rapid reproduction, and strong ability to adapt to the environment. Some pathogenic microorganisms invade the human body through direct contact or the surrounding environment, which seriously threatens human health and interferes with human normal life. As a necessities of human life, textiles are very easy to breed bacteria and be contaminated with microorganisms such as mites that endanger human health due to their own structural problems. Coupled with the surface temperature, humidity, oil, and sweat of the human body, natural conditions are created for the reproduction of microorganisms. With the development of society and the advancement of science and technology, people's demand for the comfort and functionality of textiles is increasing, so some textiles with special functions are favored by consumers. With the introduction and rapid development of the concept of deep learning, people use some of its algorithms and features to apply deep learning technology to antibacterial and antimite nanoclothing. Through these algorithms, the antibacterial and antimite properties of nanocomposites are more deeply recognized.

Because nanocomposite materials have the characteristics of antibacterial, antimite, nontoxic, tasteless, and strong stability, clothing fabrics have also begun to use this special material. This has made a significant contribution to the promotion of the textile industry. The use of deep learning, a multilayer neural network learning algorithm, to explore the antibacterial and antimite effect of clothing nanometers better demonstrates the benefits of nanocomposite materials used in clothing fabrics.

The following related researches on deep learning and antibacterial and antimite composite nanomaterials were found through sorting out. Dong Y has summarized recent advances in deep learning-based acoustic models under his

research and investigated the motivations and insights behind the techniques. Models such as recurrent neural networks U+0028 RNNs U+0029 and convolutional neural networks U+0028 CNNs U+0029, which can effectively utilize variable-length contextual information, were discussed, as well as their various combinations with other models. Then, the end-to-end optimized model was described, focusing on feature representations learned jointly with the rest of the system, connectionist temporal classification U+0028 CTC U+0029 standard, and attention-based sequence-to-sequence translation models. Robustness issues in speech recognition systems were further elaborated, and acoustic model adaptation, speech enhancement, and separation, and robustness training strategies were discussed [1]. Oshea T proposed and discussed several new applications of deep learning at the physical layer. A fundamentally new approach was developed by interpreting the communication system as an autoencoder. It shows how to extend this idea to networks of multiple transmitters and receivers and presents the concept of radio transformer networks as a means of incorporating expert domain knowledge into machine learning models. Finally, the application of convolutional neural networks on raw IQ samples for modulation classification is shown. Its accuracy is competitive compared to traditional schemes relying on expert features [2]. Kermany D S has built a deep learning framework-based diagnostic tool for screening patients with common treatable blinding retinal diseases. It used transfer learning to train neural networks with a fraction of the data of traditional methods. This approach can be applied to a data set of optical coherence tomography images, demonstrating comparable performance to human experts in classifying age-related macular degeneration and diabetic macular edema. By highlighting the regions identified by the neural network, a more transparent and interpretable diagnosis can be provided. This further demonstrated the general applicability of the artificial intelligence system in diagnosing pediatric pneumonia using chest X-ray images. This tool may ultimately help to expedite the diagnosis and referral of these treatable diseases, thereby facilitating early treatment and thus improving clinical outcomes [3]. Ravi D provided a comprehensive up-to-date review of research employing deep learning in health informatics. A critical analysis of the technology's relative merits, potential pitfalls, and future prospects is presented. They mainly focused on key applications of deep learning in translational bioinformatics, medical imaging, pervasive sensing, medical informatics, and public health [4]. Wang D L summarized the recent research progress of deep learning-based supervised speech separation. First, the background of speech separation and the concept of supervised separation are introduced. Then, it discusses the three main components of supervised separation: learning machine, training target, and acoustic features. Most of the overview is about separation algorithms and reviewing monophonic approaches, including speech enhancement (speech-nonspeech separation), speaker separation (multi-speaker separation), and speech deredundancy, as well as multimicrophone techniques. Generalization problems specific to supervised learning are discussed. They provided a historical perspective on how progress was made [5]. Cheng C showed that functional graphene nanomaterials (FGNs) are an emerging material. It has extremely unique physical and chemical properties and physiological capabilities to interfere with and/or interact with biological organisms. Therefore, FGN offers multiple possibilities for various biological applications. In addition to their use in drug/gene delivery, phototherapy, and bioimaging, recent studies have shown that FGNs can significantly facilitate interfacial biological interactions, especially with proteins, mammalian cells/stem cells, and microbes. FGNs can adsorb and concentrate nutritional factors including proteins in physiological media. In addition, FGNs can also interact with cocultured cells through physical or chemical stimulation, thereby significantly modulating their cell signaling and biological properties [6]. Shivakumar D T demonstrated that metallization layers of aluminum, gold, or copper can be prevented from interacting with silicon substrates by thin boron layers grown by chemical vapor deposition (CVD) at 450°C. A 3-nm-thick boron layer was investigated in detail. It forms the p-anode region of the PureB diode with zero metallurgical junction depth on the n-type silicon. Metals were deposited by electron beam-assisted physical vapor deposition (EBPVD) at room temperature. It is annealed at temperatures up to 500°C. In all cases, the B layer is an effective material barrier between metal and silicon. The almost unchanged I–V characteristics of the PureB diodes and the microscopy of the deposited layers were examined and verified. In order to obtain this result, it is required that the silicon surface must be cleaned before B deposition. Otherwise, any silicon surface contamination will prevent complete B coverage, resulting in increased current flow, sometimes Schottky-like. For Au, the room temperature interaction with Si is excessive through such pinholes in the B layer after annealing at 500°C [7]. These documents are very detailed for the introduction of deep learning and nanomaterials and have great reference value for the writing of this article.

In this paper, the antibacterial and antimite properties of nanocomposites under different conditions were explored through deep learning methods. And during the experiment, it was found that the ATA nanocomposite is the most suitable for clothing fabrics. Under the same conditions, compared with elemental Ag nanomaterials, ATA has stronger stability and antimite and antibacterial properties, and the cost of using materials is lower.

2. Method of Nanometer Antimite and Antibacterial for Clothing Based on Deep Learning

Research on deep learning has a long history. Deep learning originated from artificial neural networks and is also classified as machine learning. Deep learning conveys image categories and features through a multilayer information network [8–10]. It is mainly used in the field of artificial intelligence and studies multiple interdisciplinary subjects, such as neural networks, image feature modeling, image recognition, and target detection. In 1943, the deep neural network based on deep learning was first proposed, and it was found that the neural network had a strong ability to learn self-features; in 1957, the perceptron model came out to deal

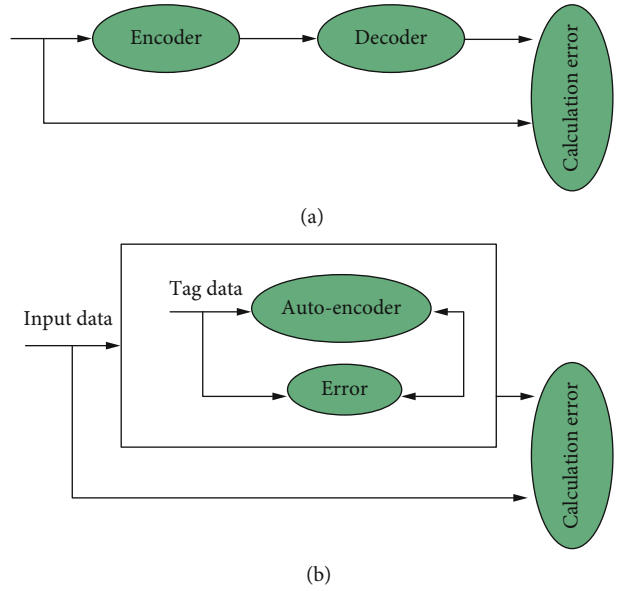

Figure 1: Unsupervised learning and supervised learning modes.

with the two-class problem; in 1986, the BP neural network based on neural network was proposed; in 2006, the concept of deep learning was first proposed; since 2014, the extensive application of deep learning in deep learning in image recognition has improved the accuracy of image recognition. With the continuous development and maturity of deep learning technology, the application of deep learning is becoming more and more extensive, and this technology is used in more and more fields.

2.1. Autoencoder. Autoencoder is an unsupervised learning algorithm that connects encoder and decoder across layers [11]. The input layer, hidden layer, and output layer constitute the autoencoder. By compressing the input data into another low-dimensional data to output the data set, it is divided into two parts: the encoder and the decoder [12]. In general, determining the expression of input data is mainly to see whether the output data is consistent with the input data. If they are inconsistent, the parameters should be adjusted so that the resulting data has the smallest error and is close to the output data and the input data [13]. The results are shown in Figure 1. The entire encoder contains two convolutional layers and one pooling layer. The convolutional layers work together to extract feature maps. The pooling layer performs downsampling and finally outputs the feature map. The decoder is the final network output. The connection layer between the encoder and the decoder mainly connects the corresponding feature maps and then becomes the data input of the next convolutional layer.

When the decoder activation function is followed by identity, the squared error function is obtained. The identity condition needs to satisfy the normal distribution:

$$Q(t, x) = t - x^2. \tag{1}$$

When the decoder activation function is a sigmoid function, the cross entropy function is obtained:

$$Q(t, x) = -\sum_{o=1}^{n} [t_o \log (x_o) + (1 - t_o) \log (1 - x_o)]. \tag{2}$$

Finally, the overall loss function is obtained:

$$K_{(AF)}(\varepsilon) = \sum_{c \in s} Q(t, g(f(t))). \tag{3}$$

2.2. Restricted Boltzmann Machine. Restricted Boltzmann machine neurons are relatively simple. It consists of two groups of neurons in the input layer and the hidden layer and is a stochastic network model [14]. Here, it is assumed that the input layer is b and the hidden layer is a. As can be seen from Figure 2, each neuron in the input layer and the hidden layer is related to each other. But if the neurons in each network model are independent, the neurons in each layer are not connected to each other [15]. Restricted Boltzmann machine has been applied in dimension reduction, classification, collaborative filtering, feature learning, and topic modeling.

The basic structure of RBM is not limited by orientation. Assuming that the values of neurons in these two layers are between 0 and 1, $k_i \in \{0, 1\}$, $m_x \in \{0, 1\}$, w and e represent the number of neurons in the input layer and hidden layer, respectively. If the specific values of the input neurons have been given, p_i is not equal to 0. The formula that will result in the combined model is

$$E(k, m, \alpha) = -\sum_{i=1}^{w} \sum_{x=1}^{e} g_{ix} k_i m_x - \sum_{i=1}^{w} p_i k_i - \sum_{x=1}^{e} q_x m_x, \tag{4}$$

where g_{ix} represents the weight coefficients of the input layer and the hidden layer; p_i represents the bias term of each neuron in the input layer; q_x represents the bias term of each neuron in the hidden layer; and α represents the grid parameter of the RBM.

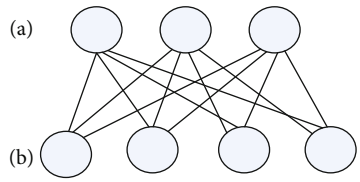

Figure 2: Restricted Boltzmann machine model.

Using the Boltzmann algorithm to determine the proportional distribution function $Z(\varepsilon)$, the formula can be obtained. Boltzmann machine is used to combine the advantages of multilayer feedforward neural network and discrete Hopfield network in network structure, learning algorithm, and dynamic operation mechanism. It is based on discrete Hopfield network and has learning ability. It can find the optimal solution through a simulated annealing process.

$$f(y,x) = \frac{1}{z(\varepsilon)} \exp\left(-E(y,x;\varepsilon)\right) = \frac{1}{z(\varepsilon)} \prod_{ij} e^{w_i y_i x_j} \prod_i e^{a_i y_i} \prod_j e^{b_j x_j}, \tag{5}$$

$$Z(\varepsilon) = \sum_y \sum_x \exp(-E(y,x;\varepsilon)). \tag{6}$$

A proportional distribution function $Z(\varepsilon)$ of t is input to the data. According to the marginal distribution of the combined probability distribution $f(y,x)$, the problems encountered in real life can be solved, and the following formula can be obtained:

$$f(t) = \frac{1}{Z(\varepsilon)} \sum_x \exp(-E(t,x;\varepsilon)). \tag{7}$$

The grid parameter ε is calculated using the RBM feature extraction method. The subsequent input data is obtained through the calculated grid parameters. It refers to the boundary of grid parameter domain calculated according to the characteristics of 3D grid (while the fixed boundary method is artificially specified). Assuming that the number of samples is W, then, the measurement method of the grid parameters is the likelihood function, and the formula is as follows:

$$\varepsilon = \arg\ \max_\varepsilon \sum_{w=1}^{W} \log\left(p\left(t^{(w)}\right)\right). \tag{8}$$

The optimal parameter ε of the network with the maximum value of the $L(\varepsilon) = \arg\ \max_\varepsilon \sum_{w=1}^{W} \log\left(p(t^{(w)})\right)$ function is measured by the method of stochastic gradient ascent (SGA). The partial derivative value of each network parameter is a $\log\left(p(t^{(w)})\right)$ function, which can be obtained by the following formula:

$$\frac{\chi l}{\chi \varepsilon} = \sum_w^W \left(\left\langle \frac{\chi\left(-E\left(t^{(q)},x\right)\right)}{\chi\varepsilon} \right\rangle_{p(\varepsilon)} - \left\langle \frac{\chi(-E(t,x))}{\chi\varepsilon} \right\rangle_{p(t,x)} \right). \tag{9}$$

When the partial derivatives of the specific parameters g_{ix}, p_i, and q_i of the likelihood function have only one simple parameter facing the training grid, the following formula can be obtained:

$$\frac{\chi p(t)}{\chi g_{ij}} = \left\langle t_i x_j \right\rangle_{p(x)} - \left\langle t_i x_j \right\rangle_{p(t,x)}, \tag{10}$$

$$\frac{\chi p(t)}{\chi (p_i)} = \left\langle t_i \right\rangle_{p(x)} - \left\langle t_i \right\rangle_{p(t,x)}, \tag{11}$$

$$\frac{\chi p(t)}{\chi (q_i)} = \left\langle t_i \right\rangle_{p(x)} - \left\langle t_i \right\rangle_{p(t,x)}. \tag{12}$$

Assuming that t_0 represents the input layer data, according to the obtained data visualization, the activation value of each hidden layer w_0 is calculated by the method of the sigmoid network activation function, and the following formula is obtained:

$$p(t_0 = 1 | w_o) = 1 / \left(1 + \exp\left(-\sum_i v_i g_{ij} + q_i\right)\right). \tag{13}$$

According to the characteristics of the symmetry of the RBM grid structure, when the hidden layer is in the active state, the activation value of the input layer can be obtained according to the following formula:

$$p(t_i = 1 | t_0) = 1 / \left(1 + \exp\left(-\sum_j t_i w_{ij} + a_j\right)\right). \tag{14}$$

2.3. Deep Belief Network. A deep belief network is a type of machine learning that consists of multiple RBM networks. It is a probabilistic generative model built between data and labels, which can be applied to both unsupervised learning and supervised learning [16–18]. RBM network consists of visible layer and hidden layer. By definition, unsupervised learning is used to deal with the sample set not marked by classification when designing the classifier. Supervised learning refers to the process of using a group of samples of known categories to adjust the parameters of the classifier to achieve the required performance, which is also called supervised training or teacher learning. The difference is that supervised learning means that a set of data is given manually and the attribute value of each data is also given. For each sample in the data set, we want the algorithm to predict and give the correct answer: regression problem and classification problem. In unsupervised learning, data is not labeled or has the same label. Its network structure is shown in Figure 3.

As can be seen from Figure 3, the deep belief network is composed of RBM structures [19]. Deep belief networks

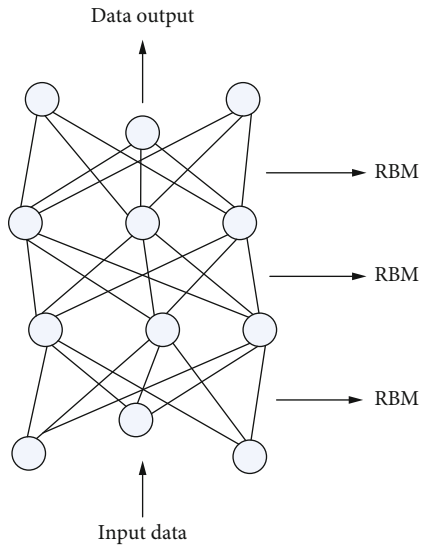

Figure 3: DBN deep learning model.

solve the difficult problem of training multilayer neural networks. It achieves data features by training the weights between each constituent neuron. The deep belief network training process is carried out step by step. In the training process of each layer of neurons, the feature image of the hidden layer is inferred through the data, and the previously obtained hidden layer is used as the data vector of the next layer to progress layer by layer, and so on. Finally, the entire deep belief network is fine-tuned through supervised learning [20]. After the above actions, a basic supervised learning algorithm is completed by concatenating the final results [21].

3. Deep Neural Network

Since the deep neural network is extended from the traditional neural network, the research of the deep neural network has not been effectively developed for a long time, and it has been in the research stage of one or two hidden layers [22]. It does not perform well in forward propagation, back propagation, and gradient descent, and is not even as good as a single hidden layer neural network. In this regard, many scholars have been exploring what causes the deep neural network to have poor ability to deal with problems [23]. At present, the methods of training neural networks are based on the idea of back propagation; that is, according to the error calculated by the loss function, the weight of the depth network is updated and optimized by gradient back propagation.

According to the answers given by most scholars, two main reasons are summarized: First, the value of the initial parameters affects the neural network, which is also the drawback of the gradient descent method. Second, the increase of grid parameters leads to an increase in the number of neural network layers. The neural network is originally a fitter, which aggravates the overfitting of the deep neural network, and the final result is not good [24]. At first, each object is regarded as a cluster, and then, these clusters are merged step by step according to some criteria. The distance between the two clusters can be determined by the similarity of the nearest data points in the two different clusters. The clustering process is repeated until all clusters meet the number of clusters.

It has been proven by practice that the weight matrix can be shifted by training the initial weights of the deep neural network step by step, which makes the in-depth study of the deep neural network go a step further. Some experts proposed to train a DBN in the forward direction based on the RBM network and then expand the DBN in the reverse direction. Finally, the whole network is regarded as a complete AE using the traditional BP algorithm for repeated training [25]. BP network can learn and store a large number of input-output mode mapping relationships without revealing the mathematical equations describing this mapping relationship in advance. In this way, AE actually becomes the first successfully trained deep autoencoder on the intelligent algorithm. The initial training process of the deep neural network is shown in Figure 4.

3.1. Convolutional Neural Network. Convolutional neural network is divided from artificial neural network, which is a multilayer neural network structure with the ability of deep learning [26]. Convolutional neural networks rely on convolutional and downsampling layers to extract data. The weight of some neurons in the same layer is the same, and it is not completely connected with neurons, but each layer has multiple neurons connected to each other [27]. The convolutional neural network is extended into two parts: The first part is the convolutional layer and the pooling layer (downsampling layer). The second part is the fully connected layer and the output layer. The input layer is where the algorithm begins to affect the entire network output value. The convolutional layer mainly plays the function of extracting features and is an important part of the entire neural network. The pooling layer samples the output data and obtains the feature map after the convolutional layer. Each neuron of the fully connected layer is connected to the neurons of the output layer to achieve the function of a classifier.

The concept of weight sharing means that the value of the local receptive field in the convolutional neural network is the same in the process of feature image generation. Neurons have the same features but recognize staggered two-dimensional planes. The weight sharing feature allows the neural elements of the neural network in a two-dimensional plane to be translated but not deformed. It also shows the same feature data during the weight sharing process.

The downsampling operation is a nonlinear dimensionality reduction operation. It can make difficult-to-recognize special images easier to identify through dimensionality reduction methods. It simplifies the entire neural network and reduces the number of neural elements in the neural network, but does not affect the final output. As shown in Figure 5, it is the basic structure of convolutional neural network.

Convolutional neural networks are more widely used in object detection. A new breakthrough has been found for improving the accuracy of target detection through the convolutional neural network method.

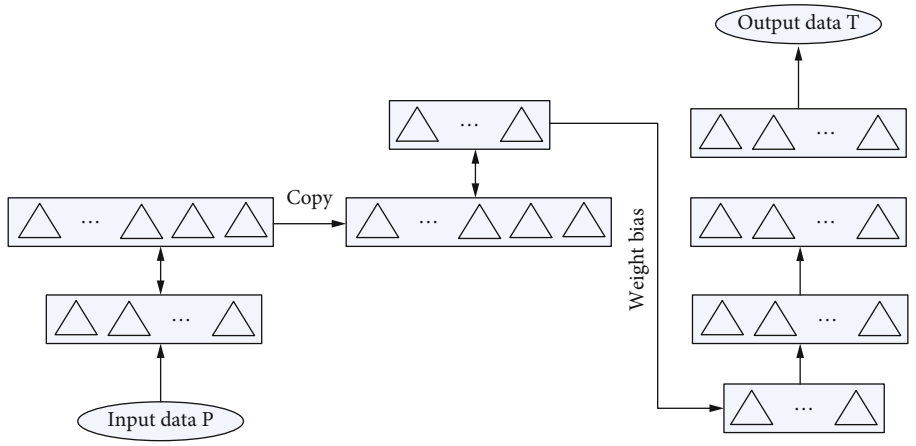

Figure 4: Pre-training process of deep neural network.

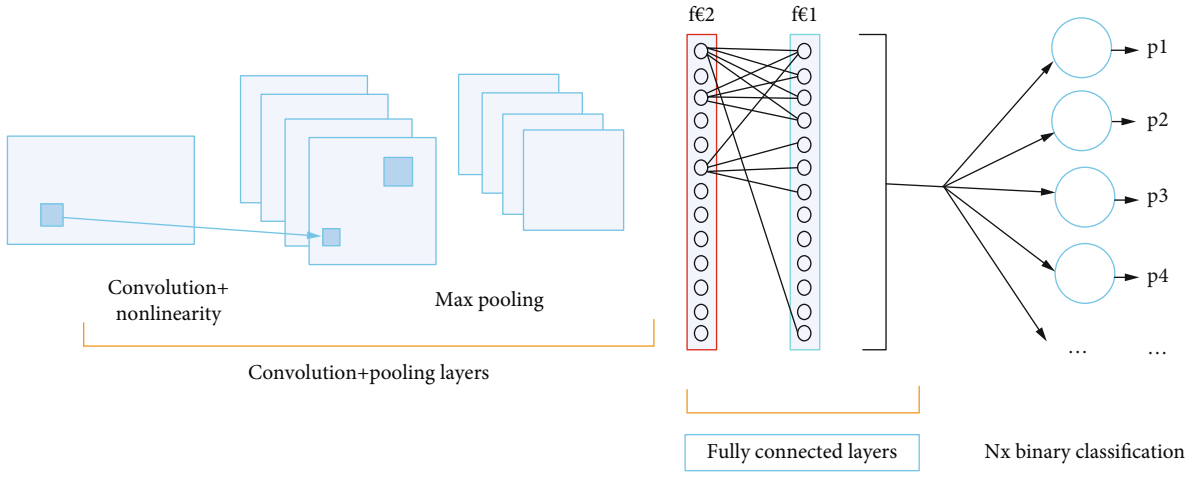

Figure 5: The structure of the convolutional neural network.

A feature map on a convolutional layer in a convolutional neural network is connected to the corresponding convolution kernel. By introducing an activation function after calculation, and then calculating the feature with the activation function, each input data can be accurately obtained [28]. The data of each output is formed by combining multiple feature maps, and the formula is obtained:

$$v_i^w = f(x_i^w), \tag{15}$$

$$x_i^w = \sum_{k \in M_i} v_i^{w-1} \cdot a_{ki}^w + r_i^w, \tag{16}$$

where v_i^w is the i-th output data of each convolutional layer w in the convolutional network; x_i^w is the activation value of the i-th layer of the w-th convolutional layer of the convolutional network; M_i is the feature data set for calculating the activation value x_i^w; $f(\bullet)$ is the activation function in the convolutional neural network; a_{ki}^w is the convolution kernel vector set in the convolutional network; and r_i^w is the final bias function of the convolutional network.

The activation function set by the pooling layer in each convolutional network is denoted by down$(\bullet)$. In each pooling layer, the output feature map convolved by each convolutional network can be obtained by the following formula:

$$x_i^w = \int_i^w \text{down}\left(v_i^{w-1}\right) + r_i^w. \tag{17}$$

In a convolutional network where each convolutional layer is connected to each other, the input of all connected convolutional layers is the combination of all 2D feature images. All input influence degree coefficients are summed by convolution. Finally, the feature output of each connected convolutional layer can be obtained by using the preset activation function, which can be obtained

$$x_i^w = m_i^w v^{w-1} + r_i^w. \tag{18}$$

According to each weight, the final output is the convolutional layer sensitivity. The object can be classified, identified, predicted, or decided according to its characteristics. In

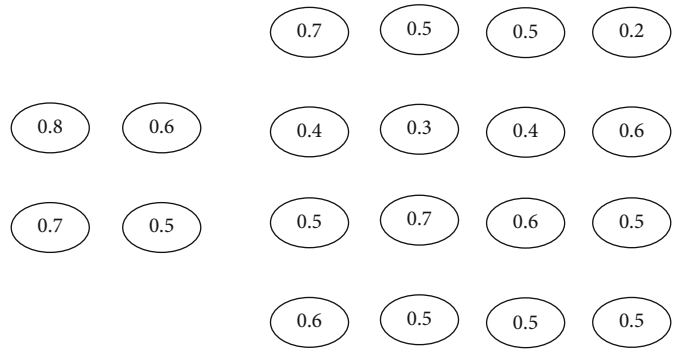

Figure 6: Upsampling operation diagram.

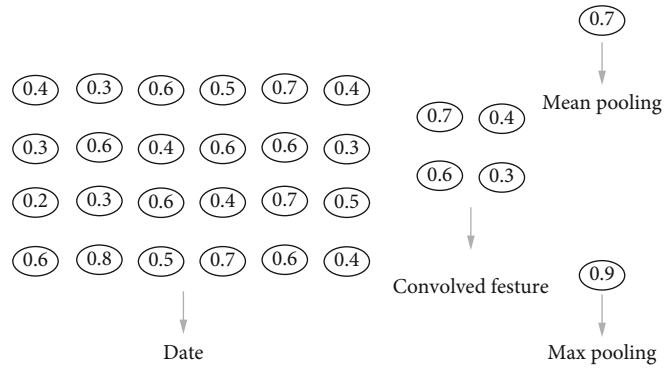

Figure 7: Schematic diagram of the operation of convolution and pooling.

this process, the most important step is feature extraction, that is, how to extract the features that can distinguish things to the greatest extent:

$$\phi_x^l = \int_x^{l+1} \left(\lambda'\left(u_x^l\right) \circ \mathrm{up}\left(\phi_x^{l+1}\right)\right). \tag{19}$$

By implementing the convolutional layer using the Kroneckers product, the function can be obtained:

$$\mathrm{up}(z) = z \otimes 1_{n\times n}. \tag{20}$$

According to the maximum pooling used above, put 4 in the model ×4 region is regarded as the set of some characteristics, that is, the set of activation values of a certain layer in the neural network. A large number means that some specific features may be detected. The features in the upper left quadrant may be a vertical edge, an eye, or cap features that people are afraid to encounter. The upsampling operation shown in Figure 6 can be obtained.

After the input image is extracted by the convolution layer image, additional image features are obtained by pooling. Figure 7 is a process diagram of image convolution and pooling.

The fully connected layer inputs a multidimensional vector. Each vector is converted into a bunch of vectors, and the sensitivity can be used to calculate the weight of each neuron. The formula for calculating the sensitivity of the fully connected layer is

$$\phi_x^l = \left(w^{l+1}\right)^R \phi^{l+1} \circ f'\left(v^l\right). \tag{21}$$

The actual training of the convolutional neural network has nothing to do with the previous input variables; it only reacts to the input variables. Because the bacteriostatic rate of ATA composites within 24 hours is constantly changing, in a day, if the time data of a certain hour of the day is randomly selected to analyze the results, the fluctuation of the data of the previous hour or the next hour will be ignored. Therefore, the change data of one day must be sampled.

4. The Research Experiment and Analysis of Nanometer Antimite and Antibacterial of Clothing Based on Deep Learning Technology

The application of nanomaterials in clothing is mainly to integrate nanomaterials into fabric fibers. For the antimite and antibacterial properties of clothing nanometers, the main method is to add substances with antibacterial properties into nanofibers. With the deepening of research, substances with antibacterial properties are mainly divided into the following two categories according to the properties of the substances: (1) Metals and metal oxides. Metal oxide antibacterial materials mainly include ZnO, TiO_2, and Fe_3O_4. (2). The surface chemical structure of house dust mite before and after ATA nanomaterial treatment showed that the structure of lipid, protein, and polysaccharide of

Table 1: Effect of load time on fabric load.

Load time	Load fabric number	Weight of fabric before load/g	Weight of fabric after load/g	Load/g	Load per 0.75 g fabric/g
	1-1	17.42	18.34	0.91	0.04
3 min	1-2	17.85	18.78	0.93	0.04
	1-3	17.22	18.12	0.91	0.04
	2-1	17.72	18.88	1.16	0.05
5 min	2-2	17.24	18.41	1.17	0.05
	2-3	17.26	18.18	1.20	0.05
	3-1	17.51	18.71	1.20	0.05
7 min	3-2	18.24	19.41	1.18	0.05
	3-3	18.42	18.42	1.18	0.05

Table 2: Antibacterial effect of *Escherichia coli* fabrics under load time.

		Under visible light			Under dark conditions		
Load time	Parallel plate number	Number of colonies/piece	Viable bacteria concentration/cfu/ml	Bacteriostatic rate/%	Number of colonies/piece	Iable bacteria concentration/cfu/ml	Bacteriostatic rate/%
3 min	1	2×10	0.020×106	99.60	5×10	0.04×106	98.88
	2	3×10	0.03×106		7×10	0.07×106	
5 min	1	0	0	100	0	0	100
	2	0	0		0	0	

Table 3: Bacteriostatic rate of *Staphylococcus aureus* at 3 min loading.

	Under visible light		Under dark conditions		
Plate number	Average number of colonies/piece	Bacteriostatic rate/%	Average number of colonies/piece	Viable bacteria concentration/cfu/ml	Bacteriostatic rate/%
1	48×10	99.96	48×10	4.80×106	99.95
2	170×10		205×10	0.021×106	

mite body wall changed; TiO2 is a typical photocatalytic antibacterial material, which has the characteristics of low toxicity, low price, acid and alkali resistance, and strong antibacterial ability under UV irradiation; and Ag ion is the most efficient metal ion antibacterial agent known at present. It has the advantages of good antibacterial effect, low antibacterial concentration, killing many kinds of bacteria, and strong drug resistance. Taking Ag, TiO_2, and ATA as research objects, their antibacterial properties were analyzed. Ag ion is a metal ion antibacterial agent that can kill many kinds of bacteria and has strong drug resistance; TiO_2 is a good photocatalyst; ATA has strong stability. The absorbance values of different materials are detected using deep learning techniques. Bacterial growth kinetics were analyzed according to the degree of change in absorbance value. The absorption coefficient is related to the wavelength of the incident light and the material passed by the light. As long as the wavelength of the light is fixed, the absorption coefficient of the same material will remain unchanged. When a beam of light passes through a light absorbing substance (usually a solution), the solute absorbs light energy and the intensity of light decreases. Absorbance is a physical quantity used to measure the degree of light absorption.

4.1. Preparation of ATA Antibacterial Fabric. 9 pieces of treated fabrics (20 cm × 20 cm) were immersed in ATA nanosolution at different times. Each corresponds to a different parallel sample. They were taken out at different times, squeezed out excess liquid, and passed through an oven drying process at 125°C for 15 minutes. Then, the change of the fabric before and after loading and the loading of the antibacterial agent of the fabric in different time periods were measured. The longer the load time, the worse the fabric load.

It can be seen from Tables 1 and 2 that in the presence of light, the antibacterial activity of ATA against *Escherichia coli* reaches 99.60% and 100% in two time periods; in the absence of light, the antibacterial activity of ATA against *Escherichia coli* reaches 99.60% and 100%. The bacteriostatic rate of the two cases is basically close to 100%, and the antibacterial effect is excellent.

According to Table 3, the antibacterial performance of *Staphylococcus aureus* is very good in the presence of light

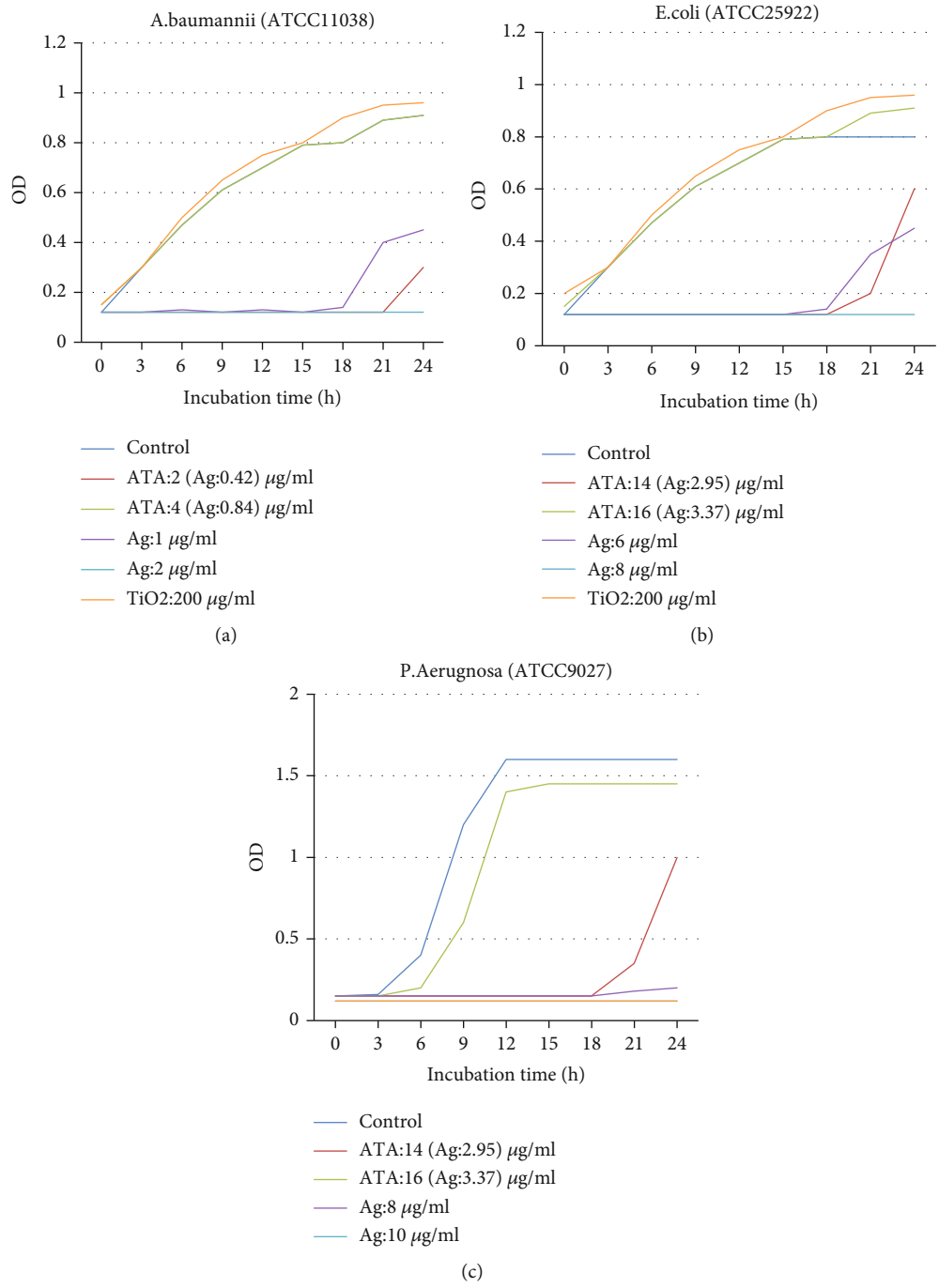

Figure 8: The analysis of the activity of ATA against Gram-negative bacteria.

or in the dark, and the bacteriostatic rate is basically close to 100%.

4.2. ATA against Gram-Negative Bacteria. The experimental objects were *Acinetobacter baumannii*, *Escherichia coli*, and *Pseudomonas aeruginosa*.

As shown in Figure 8, the minimum inhibitory concentration values of ATA against Gram-negative bacteria are: *Acinetobacter baumannii* was 10 μg/ml. *Escherichia coli* was 16 μg/ml. *Pseudomonas aeruginosa* is 16 μg/ml. Ag concentrations in ATA were 2.11, 3.37, and 3.37 μg/ml. The minimum inhibitory concentrations corresponding to elemental Ag were 4, 8, and 10 μg/ml. And 200 μg/ml still has only weak antibacterial effect. The results of the minimum inhibitory concentration test showed that ATA has strong antibacterial ability against all the tested strains. With the increase of ATA and Ag concentrations, its antibacterial activity was enhanced, and the reproduction and growth rate of all bacteria slowed down rapidly.

4.3. ATA against Gram-Positive Bacteria. The experimental subjects were *Streptococcus pneumoniae*, *Staphylococcus*

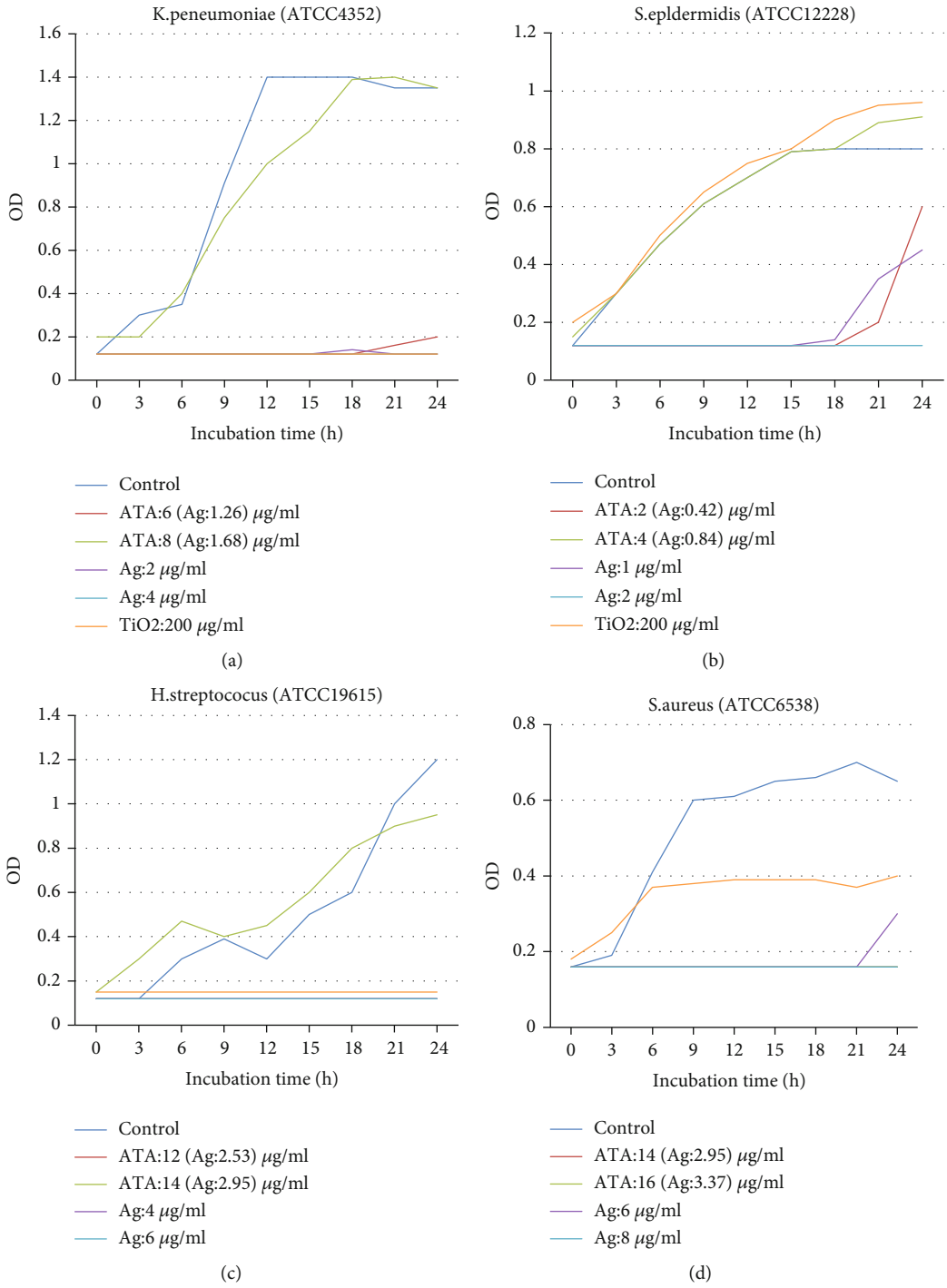

Figure 9: The analysis of ATA against Gram-positive bacteria.

epidermidis, *Streptococcus hemolyticus*, and *Staphylococcus aureus*.

Figure 9 shows that the minimum inhibitory concentrations of ATA against Gram-positive bacteria were 4 μg/ml for *Streptococcus pneumoniae*, 8 μg/ml for *Staphylococcus epidermidis*, 14 μg/ml for *Streptococcus hemolyticus*, and 16 μg/ml for *Staphylococcus aureus*. ml. The Ag concentrations in ATA were 0.84, 1.68, 2.95, and 3.37 μg/ml, respectively; the minimum inhibitory concentrations corresponding to elemental Ag were 2, 4, 6, and 8 μg/ml. 200 μg/ml TiO_2 has only weak antibacterial effect on all the above bacteria. At the minimum inhibitory concentration, the content of Ag in ATA was about 1/2 to 1/3 of that of elemental Ag. That is to say, ATA not only has powerful broad-spectrum antibacterial properties, but also greatly reduces the use of Ag and achieves the purpose of saving precious metal Ag. Even if the concentration of pure TiO_2 reaches 200 μg/ml, there is only a weak antibacterial effect. These results imply the occurrence of synergistic antibacterial

Table 4: Comparison of minimum inhibitory concentrations of TiO_2, Ag and Ag/TiO_2.

Bacterial species and number	Gram species (negative-; positive +)	TiO_2 minimum inhibitory concentration (μg/ml)	Ag minimum inhibitory concentration (μg/ml)	ATA minimum inhibitory concentration (μg/ml)
A. baumannii	—	More than 200	4	10 (Ag:2.11; TiO2:7.89)
E. coli	—	More than 200	8	16 (Ag:3.37; TiO2:12.63)
P. aeruginosa	—	More than 200	10	16 (Ag:3.37; TiO2:12.63)
S. pneumoniae	+	More than 200	2	4 (Ag:0.84; TiO2:3.16)
S. epidermidis	+	More than 200	4	8 (Ag:.68; TiO2:6.32)
S. hemolyticus	+	More than 200	6	14 (Ag:2.95; TiO2:11.05)
S. aureus	+	More than 200	8	16 (Ag:3.37, TiO2:12.63)

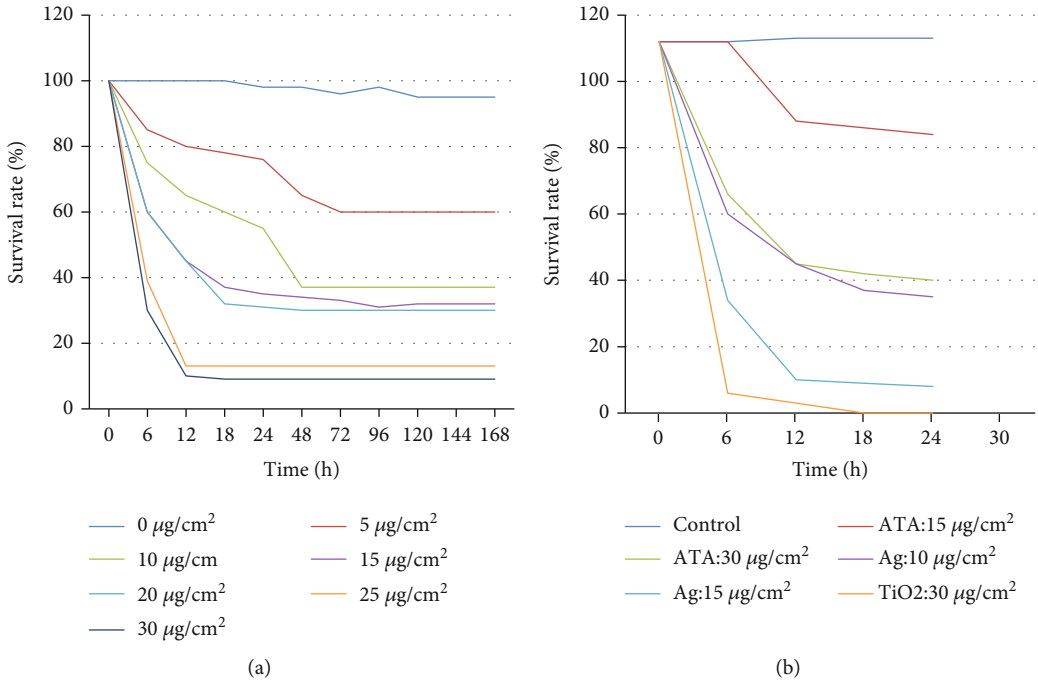

Figure 10: The relationship between the antihouse dust mite activity and time of the samples at different concentrations.

properties of ATA, possibly because Ag and TiO_2 have different antibacterial action mechanisms. In addition, the minimum inhibitory concentration of ATA was lower than that of other inorganic antibacterial materials. Table 4 is the comparative data of minimum inhibitory concentration of TiO_2, Ag, and Ag/TiO_2.

Through experiments, it was found that adding different amounts of TiO_2 to the nanomaterials can effectively inhibit the activity and survival rate of bacteria. Its main antibacterial mechanism is that TiO_2 kills bacteria by destroying their cell walls. Compared with Ag nanomaterials, ATA nanometers have small particle size and strong stability. Under the same dosage, the Ag concentration in ATA is about 1/2-1/3 of that of elemental Ag, which saves the cost of Ag to a great extent.

4.4. Antimite Activity Analysis of ag/TiO_2. The antimite activity of ATA against house dust mites was evaluated by the method of deep learning technology. It can be seen from Figure 10 that ATA has a strong ability to remove mites. According to the treatment of house dust mites with different doses of ATA, the survival rates of house dust mites after 24 hours were 76%, 46%, 33%, 27%, 5%, and 2%, respectively. When the time was extended to seven days (168 h), the survival rate of house dust mites did not change significantly, but only slightly decreased. As can be seen from Figure 10, ATA, Ag, and TiO_2 have obvious antimite effects within 24 hours, and the effect is not so obvious after 24 hours, and ATA has a synergistic antimite effect.

5. Discussion

This paper mainly discusses and studies the antimite and antibacterial effect of clothing nanometers based on deep learning technology. In this paper, the antibacterial and antimite effects of Ag, TiO_2 and Ag/TiO_2 (ATA) nanocomposites were experimentally studied by using deep learning algorithm. It compares the antibacterial and antimite properties of different composite nanomaterials under different conditions. According to the experiments, the nanomaterials with the strongest antibacterial properties and the most suitable for integration into clothing fabrics are obtained. The

experimental results show that the deep learning technology can be used in the research on the antibacterial and antimite of clothing nanometers. And under this technology, the antimite and antibacterial experiments of nanomaterials have obtained satisfactory results.

6. Conclusions

Ag, TiO_2, and Ag/TiO_2 (ATA) nanocomposites have certain antimite and antibacterial effects and are widely used. However, the Ag/TiO_2 (ATA) nanocomposites prepared by Ag and TiO_2 have stronger stability and better antibacterial properties. With the advancement of social technology, Ag/TiO_2 (ATA) nanocomposites are used more and more widely as a bacteriostatic agent, and the development prospect is getting better and better. The synergistic antimite effect of ATA was obtained by evaluating the antimite activity of ATA against house dust mites by using deep learning technology. Within 24 hours, TA, Ag, and TiO_2 had obvious antimite effects during this period.

Data Availability

The data that support the findings of this study are available from the corresponding author upon reasonable request.

Conflicts of Interest

The authors declared no potential conflicts of interest with respect to the research, author-ship, and/or publication of this article.

References

[1] Y. Dong and J. Li, "Recent progresses in deep learning based acoustic models," *IEEE/CAA Journal of Automatica Sinica*, vol. 4, no. 3, pp. 396–409, 2017.

[2] T. Oshea and J. Hoydis, "An introduction to deep learning for the physical layer," *IEEE Transactions on Cognitive Communications & Networking*, vol. 3, no. 4, pp. 563–575, 2017.

[3] D. S. Kermany, M. Goldbaum, and I. W. Ca, "Identifying medical diagnoses and treatable diseases by image-based deep learning," *Cell*, vol. 172, no. 5, pp. 1122–1131.e9, 2018.

[4] D. Ravi, C. Wong, F. Deligianni et al., "Deep learning for health informatics," *IEEE Journal of Biomedical & Health Informatics*, vol. 21, no. 1, pp. 4–21, 2017.

[5] D. L. Wang and J. Chen, "Supervised speech separation based on deep learning: an overview," *IEEE/ACM Transactions on Audio, Speech, and Language Processing*, vol. 1, no. 99, pp. 1–1, 2017.

[6] C. Cheng, S. Li, A. Thomas, N. A. Kotov, and R. Haag, "Functional graphene nanomaterials based architectures: biointeractions, fabrications, and emerging biological applications," *Chemical Reviews*, vol. 117, no. 3, pp. 1826–1914, 2017.

[7] D. T. Shivakumar, T. Kneevi, and L. K. Nanver, "Nanometer-thin pure boron CVD layers as material barrier to Au or Cu metallization of Si," *Journal of Materials Science: Materials in Electronics*, vol. 32, no. 6, pp. 1–13, 2021.

[8] R. Surendran, O. I. Khalaf, and C. Andres, "Deep learning based intelligent industrial fault diagnosis model," *CMC-Computers, Materials & Continua*, vol. 70, no. 3, pp. 6323–6338, 2022.

[9] H. Lu, Q. Liu, X. Liu, and Y. Zhang, "A survey of semantic construction and application of satellite remote sensing images and data," *Journal of Organizational and End User Computing (JOEUC)*, vol. 33, no. 6, pp. 1–20, 2021.

[10] G. Suryanarayana, K. Chandran, O. I. Khalaf, Y. Alotaibi, A. Alsufyani, and S. A. Alghamdi, "Accurate magnetic resonance image super-resolution using deep networks and Gaussian filtering in the stationary wavelet domain," *IEEE Access*, vol. 9, pp. 71406–71417, 2021.

[11] B. A. Palmer, D. Gur, S. Weiner, L. Addadi, and D. Oron, "The organic crystalline materials of vision: structure–function considerations from the nanometer to the millimeter scale," *Advanced Materials*, vol. 30, no. 41, p. 1800006.1-1800006.10, 2018.

[12] N. Akhtar and A. Mian, "Threat of adversarial attacks on deep learning in computer vision: a survey," *IEEE Access*, vol. 6, pp. 14410–14430, 2018.

[13] T. Kooi, G. Litjens, and B. V. Ginneken, "Large scale deep learning for computer aided detection of mammographic lesions," *Medical Image Analysis*, vol. 35, pp. 303–312, 2017.

[14] S. Dörner, S. Cammerer, J. Hoydis, and S. Ten Brink, "Deep learning-based communication over the air," *IEEE Journal of Selected Topics in Signal Processing*, vol. 1, no. 1, pp. 132–143, 2017.

[15] X. Wang, L. Gao, and S. Mao, "CSI phase fingerprinting for indoor localization with a deep learning approach," *IEEE Internet of Things Journal*, vol. 3, no. 6, pp. 1113–1123, 2016.

[16] G. B. Goh, N. O. Hodas, and A. Vishnu, "Deep learning for computational chemistry," *Journal of Computational Chemistry*, vol. 38, no. 16, pp. 1291–1307, 2017.

[17] S. N. Alsubari, S. N. Deshmukh, A. A. Alqarni et al., "Data analytics for the identification of fake reviews using supervised learning," *CMC-Computers, Materials & Continua*, vol. 70, no. 2, pp. 3189–3204, 2022.

[18] M. Fanqi, C. Wenying, and W. Jingdong, "Semi-supervised software defect prediction model based on tri-training," *KSII Transactions on Internet and Information Systems*, vol. 15, no. 11, pp. 4028–4042, 2021.

[19] N. Kussul, M. Lavreniuk, S. Skakun, and A. Shelestov, "Deep learning classification of land cover and crop types using remote sensing data," *IEEE Geoscience and Remote Sensing Letters*, vol. 14, no. 5, pp. 778–782, 2017.

[20] A. K. Gorshenin, V. Y. Korolev, and A. M. Tursunbaev, "Median modifications of the EM-algorithm for separation of mixtures of probability distributions and their applications to the decomposition of volatility of financial indexes," *Journal of Mathematical Sciences*, vol. 227, no. 2, pp. 176–195, 2017.

[21] F. Gu, H. Zhang, W. Wang, and S. Wang, "An expectation-maximization algorithm for blind separation of Noisy mixtures using Gaussian mixture model," *Circuits, Systems, and Signal Processing*, vol. 36, no. 7, pp. 2697–2726, 2017.

[22] W. Fu, J. Chen, and Y. Bo, "Source recovery of underdetermined blind source separation based on SCMP algorithm," *IET Signal Processing*, vol. 11, no. 7, pp. 877–883, 2017.

[23] T. Zeng and C. Liu, "A two-stage separation algorithm for weak correlation source signals," *Wireless Personal Communications*, vol. 117, no. 3, pp. 2441–2452, 2021.

[24] C. Chen and W. K. Kim, "The application of micro-CT in egg-laying hen bone analysis: introducing an automated bone

separation algorithm," *Poultry Science*, vol. 99, no. 11, pp. 5175–5183, 2020.

[25] H. Elfaig, W. Elsayed, and H. Ahmed, "Preparation and characterization of chitosan/silver nano-composite and its application on Nile water as antibacterial materials," *MRS Advances*, vol. 5, no. 26, pp. 1331–1338, 2020.

[26] F. Karabudak, R. Yesildal, and E. E. Sukuroglu, "An investigation of corrosion resistance and antibacterial sensitivity properties of nano-Ag-doped TiO_2 coating and TiO_2 coating grown on NiTi alloy with the micro-arc oxidation process," *Arabian Journal for Science and Engineering*, vol. 42, no. 6, pp. 2329–2339, 2017.

[27] Y. Choi, J. Jang, H. J. Koo, M. Tanaka, K. H. Lee, and J. Choi, "Alginate-chitosan hydrogel patch with beta-glucan nanoemulsion for antibacterial applications," *Biotechnology and Bioprocess Engineering*, vol. 26, no. 1, pp. 71–77, 2021.

[28] Y. Liu, Q. Q. Li, H. Zhang, S. P. Yu, L. Zhang, and Y. Z. Yang, "Research progress on the use of micro/nano carbon materials for antibacterial dressings," *New Carbon Materials*, vol. 35, no. 4, pp. 323–335, 2020.